# New route toward building active ruthenium nanoparticles on ordered mesoporous carbons with extremely high stability

Ying Yang[1], Chengjun Sun[2], Yang Ren[2], Shijie Hao[1] & Daqiang Jiang[1]

[1]State Key Laboratory of Heavy Oil Processing, China University of Petroleum, Changping, Beijing 102249, China

[2]X-ray Science Division, Argonne National Laboratory, 9700 S. Cass Ave., Argonne, Illinois 60439, USA

## Table of contents

multi-component self-assembly process. Note: some ions were obliterated for clarity

**Supplementary Figure S8.** HAADF images and the corresponding particle size distributions for (a,e) 6.0%Ru-OMC, (b,f) 3.0%Ru-OMC, (c,g) 1.5%Ru-OMC and (d,h) 0.5%Ru-OMC

**Supplementary Figure S9.** Normalized EXAFS (Ru K-edge scan) plotted as $k^2$chi(k) *vs* k for (a) 3.0%Ru-$C_{16}$SC, (b) 3.0%Ru-OMSC, (c) 3.0%Ru-OMC and (d) Ru foil

**Supplementary Figure S10.** FT-IR spectra of (a) 3.0%Ru-$C_{16}$SC, (b) 3.0%Ru-OMCS and (c) 3.0%Ru-OMC

**Supplementary Figure S11.** TEM images and the corresponding EDX results for (a,b) 3.0%Ru-OMSC and (c,d) 3.0%Ru-OMC

**Supplementary Figure S12.** SEM images of (a) 3.0%Ru-$C_{16}$SC, (b) 3.0%Ru-OMCS and (c) 3.0%Ru-OMC

**Supplementary Figure S13.** Typical HAADF image of 3.0%Ru-OMC after 23 cycles

## Section S1. Chemicals and reagents

All chemicals are of analytical grade and used as received without any further purification. Cetyltrimethylammonium bromide (CTAB), tetramethoxysilane (TMOS), chitosan, 8-quinolinol, ruthenium trichloride trihydrate ($RuCl_3 \cdot 3H_2O$), concentrated hydrochloric acid (38%), formaldehyde (37%), triethylamine, zinc chloride hexahydrate, acetic acid, sodium hydroxide, acetone and ethanol are commercially available.

## Section S2. Synthetic procedures

The synthetic procedure for 5-chloromethyl-8-quinolinol hydrochloride and 8-quinolinol modified chitosan was depicted in Supplementary Fig. S1.

**Preparation of 5-chloromethyl-8-quinolinol hydrochloride.** A mixture of 5.84 g (40.0 mmol) of 8-quinolinol, 50 ml of concentrated hydrochloric acid and 6.4 ml of 37% formaldehyde was treated with 0.6 g of zinc chloride and stirred overnight. The mixture was filtered, washed with copious acetone and dried to give the title compound **1** as a yellow solid (8.32 g, 90%). Found: C, 52.44; H, 3.86; N, 5.84%. Calc. for $C_{10}H_8NOCl \cdot HCl$: C, 52.17; H, 3.91; N, 6.08%. $^1H$ NMR ($D_2O$, TMS, δ ppm): 9.24 (1H, d, C(2)H), 8.96 (1H, m, C(4)H), 8.06 (1H, m, C(3)H), 7.68 (1H, s, C(6)H), 7.36 (1H, s, C(7)H), 5.03 (2H, s, $CH_2Cl$) (Supplementary Fig. S2). UV-vis, λ (nm): 258, 313, 376 (Supplementary Fig. S3). FTIR (KBr pellets, $cm^{-1}$): 3310br (OH), 1627m (C=C), 1594s (C=N), 1550vs (aromatic), 1390s (C-N), 1087w (C-O), 819m and 769m (C-H), 694m (C-Cl) (Supplementary Fig. S4).

**Preparation of 8-quinolinol modified chitosan.** 0.9 g of chitosan (CTS) was mixed with 50 ml of 20 wt% acetic acid, and stirred for 1 h. Then 4.6 g of **1** combined with 60 ml 36 wt% triethylamine was added and stirred at 75 $^oC$ for further 36 h. The

resulting mixture was filtered, washed with ether, ethanol and water, and dried to give the light yellow solid, CTS-HQ. UV-vis, λ (nm): 254, 336, 425 (Supplementary Fig. S5). FTIR (KBr pellets, $cm^{-1}$): 3063 (NH), 2921, 2863 ($CH_2$), 1623 (C=N), 1580, 1507, 1740, 1418, 1365 (Ph), 1265, 1228, 1197, 1155, 1113, 1070, 891, 828, 781, 703 (Supplementary Fig. S6)

**Synthesis of 3.0%Ru-C.** The 3.0%Ru-C was prepared by direct carbonization of chitosan-ruthenium coordination polymers in the absence of silica and surfactant. The chitosan-ruthenium coordination polymer was first synthesized by mixing and stirring CTS-HQ and $RuCl_3 \cdot 3H_2O$ (1 CTS-HQ: 0.125 Ru) at room temperature for 1 h, and the resulting solid was filtered, washed, dried and further pyrolysed using the temperature program mentioned in the manuscript, giving 3.0% Ru-C.

## Section S3. Characterization information

The Ru-containing sample mixed with boron nitride was pressed into a self-supporting disk and measured. All samples were scanned a minimum of three times. Ru metal powder (Aldrich, 99.99%) was used as a reference for the Ru K-edge scan. The X-ray absorption fine structure (XAFS) data were processed using the Athena software for background removal, post-edge normalization and XANES analysis. The oxidation states of the samples were determined by comparing the inflection point of the edge from the sample to that of standards with known oxidation state. The EXAFS was analyzed using Artemis software, which implemented FEFF. The EXAFS data reduction was conducted by utilizing the standard procedures. The EXAFS function, χ, was obtained by subtracting the post-edge background from the overall absorption and then normalized with respect to the edge jump step. The normalized χ(E) was transformed from energy space to k space, where k is the

photoelectron wave vector of X-rays. The χ(k) data were multiplied by $k^2$ to compensate the damping of EXAFS oscillations in the high k region. Subsequently, $k^2$-weighted χ(k) data in k space were Fourier transformed to r space to separate the EXAFS contributions from the different coordination shells. A nonlinear least-squares algorithm was applied to the curve fitting of EXAFS data in r space between 0.5 and 3.3 Å for the Ru centre depending on the bond to be fitted.

The infrared spectra (IR) of samples were recorded in KBr disks using a NICOLET 6700 spectrometer. UV-vis spectra were recorded on a Perkin Elmer spectrophotometer Lambda 650s using barium sulfate as the standard in the range 200-800 nm. Liquid $^1$H NMR spectrum was recorded on a Varian Mercury-300 MHz instrument using tetramethylsilane (TMS) as the internal standard.

**Section S4. Illustrations about cubic *Ia3d* mesophase formation**

Generalized liquid crystal templating mechanism can help understand the mesophase formation. The packing parameters ($g$) of ionic surfactants are commonly used in predicting and explaining the final mesostructures[1]. The calculation of $g$ value is simple but of great significance and guidance: $g = V/(a_0 l)$. Here, $V$ is the total volume of surfactant hydrophobic chains plus any co-solvent (organic molecules) between the chains, $a_0$ is the effective hydrophilic head group area at the aqueous-micelle surface, and $l$ is the kinetic surfactant tail length. The expected mesophase sequence as a function of $g$ value is cubic (*Pm3n*, *etc.*) and 3D hexagonal (*P63/mmc*) with $g < 1/3$, 2D hexagonal (*p6mm*) with $1/3 < g < 1/2$, cubic (*Ia3d*) with $1/2 < g < 2/3$, and lamellar with $g = 1$. In our experiment, 8-quinolinol modified chitosan (CTS-HQ) is deprotonated under the basic condition, and can interact with the cationic surfactants (CTAB) to form ion pairs to act as a co-surfactant (Supplementary Fig. S7), consistent

with the fact reported that the chitosan acts as a structure directing agent for silica synthesis at proper pH value[2]. The co-surfactant effect renders the enlargement of hydrophobic volume of the surfactant, which decreases the interfacial curvature around the surfactant micelles, thus increases *g* value, and assists the phase transformation from *p6mm* to *Ia3d*. So it is reasonable that the CTS-HQ was directed to the *Ia3d* mesophase in this study due to its templating role, rather than the commonly reported *p6mm* mesophase formed by CTAB-directed self-assembly of other organic precursors under basic conditions[3-5].

## References


1. Wan, Y. & Zhao, D. Y. On the controllable soft-templating approach to mesoporous silicates. *Chem. Rev.* **107,** 2821-2860 (2007).
2. Wang, L. X. *et al.* Effects of CTAB on porous silica templated by chitosan. *J. Mater. Sci.* **45,** 4470-4479 (2010).
3. Corma, A., Das, D., García, H. & Leyva, A. A. Periodic mesoporous organosilica containing a carbapalladacycle complex as heterogeneous catalyst for suzuki cross-coupling. *J. Catal.* **229,** 322-331 (2005).
4. Bahuleyan, B. K. *et al.* One-pot synthesis of spherical periodic mesoporous organosilica supported catalyst bearing Ni(II) α-diimine complexes for ethylene polymerization. *Catal. Commun.* **11,** 252-256 (2009).
5. Yang, Y., Zhang, Y., Hao, S. J. & Kan, Q. B. Periodic mesoporous organosilicas with bis(8-quinolinolato)dioxomolybdenum(VI) inside the channel walls. *J. Colloid Interface Sci.* **362,** 157-163 (2011).

**Supplementary Table S1** Textual properties of various samples

| Materials | $S_{BET}$[a] ($m^2\ g^{-1}$) | $S_{micro}$ ($m^2\ g^{-1}$) | $S_{meso}/S_{micro}$ | $V_t$[b] ($cm^3\ g^{-1}$) | $V_{micro}$ ($cm^3\ g^{-1}$) | $V_{meso}/V_{micro}$ | $D_p$[c] (nm) | $A_o$[d] (nm) | W[e] (nm) |
|---|---|---|---|---|---|---|---|---|---|
| 3.0%Ru-OMSC | 152.0 | 88.8 | 0.72 | 0.1174 | 0.0370 | 2.17 | 4.30 | 9.61 | 0.96 |
| 3.0%Ru-OMC | 610.7 | 323.9 | 0.88 | 0.5334 | 0.1217 | 3.55 | 4.32 | 8.81 | 0.69 |
| 3.0%Ru-C | 234.8 | 193.0 | - | 0.1215 | 0.0919 | - | - | - | - |

[a] The BET surface areas were obtained from the adsorption branches in the relative pressure range of 0.05-0.20.

[b] The single point adsorption total pore volume was taken at the relative pressure of 0.99.

[c] The pore size distributions were calculated from the desorption branches by the Barret-Joyner-Halenda (BJH) method.

[d] $A_o$ is the unit cell parameter, and $A_o = 6^{1/2}d_{211}$.

[e] Wall thickness = $A_o/3.0919 - D_p/2$.

**Supplementary Table S2** Screening of reaction conditions over 3.0%Ru-OMC

| Entry | Catalyst amount (wt%) | $H_2$ pressure (MPa) | Reaction time (h) | Temperature ($^oC$) | LA conversion[a] (%) | GVL yield (%) |
|---|---|---|---|---|---|---|
| 1 | 5 | 4.5 | 3.5 | **130** | 60.2 | 55.0 |
| 2 | 5 | 4.5 | 3.5 | **150** | 100 | 95.8 |
| 3 | 5 | 4.5 | 3.5 | **180** | 100 | 94.2 |
| 4 | **1** | 4.5 | 3.5 | 150 | 98.0 | 98.0 |
| 5 | **0.5** | 4.5 | 3.5 | 150 | 98.4 | 98.4 |
| 6 | **0.2** | 4.5 | 3.5 | 150 | 98.0 | 98.0 |
| 7 | **0.1** | 4.5 | 3.5 | 150 | 66.6 | 66.6 |

| | | | | | | |
|---|---|---|---|---|---|---|
| 8 | 0.2 | 4.5 | **4.0** | 150 | 100 | 85.0 |
| 9 | 0.2 | 4.5 | **3.0** | 150 | 100 | 92.4 |
| 10 | 0.2 | 4.5 | **2.0** | 150 | 100 | 95.0 |
| 11 | 0.2 | 4.5 | **1.5** | 150 | 97.0 | 93.6 |
| 12 | 0.2 | 4.5 | **1.0** | 150 | 90.8 | 80.0 |
| 13 | 0.2 | **3.0** | 2 | 150 | 83.3 | 77.3 |
| 14 | 0.2 | **1.5** | 2 | 150 | 45.6 | 51.0 |
| 15 | **0.3** | 4.5 | 2 | 150 | 99.4 | 98.8 |

[a] Reaction condition: 5.0 g of LA without solvent.

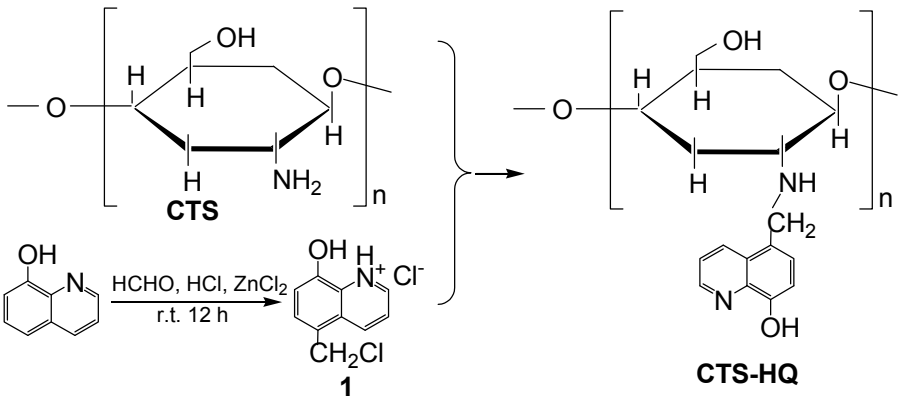


**Supplementary Figure S1.** Synthesis of CTS-HQ.

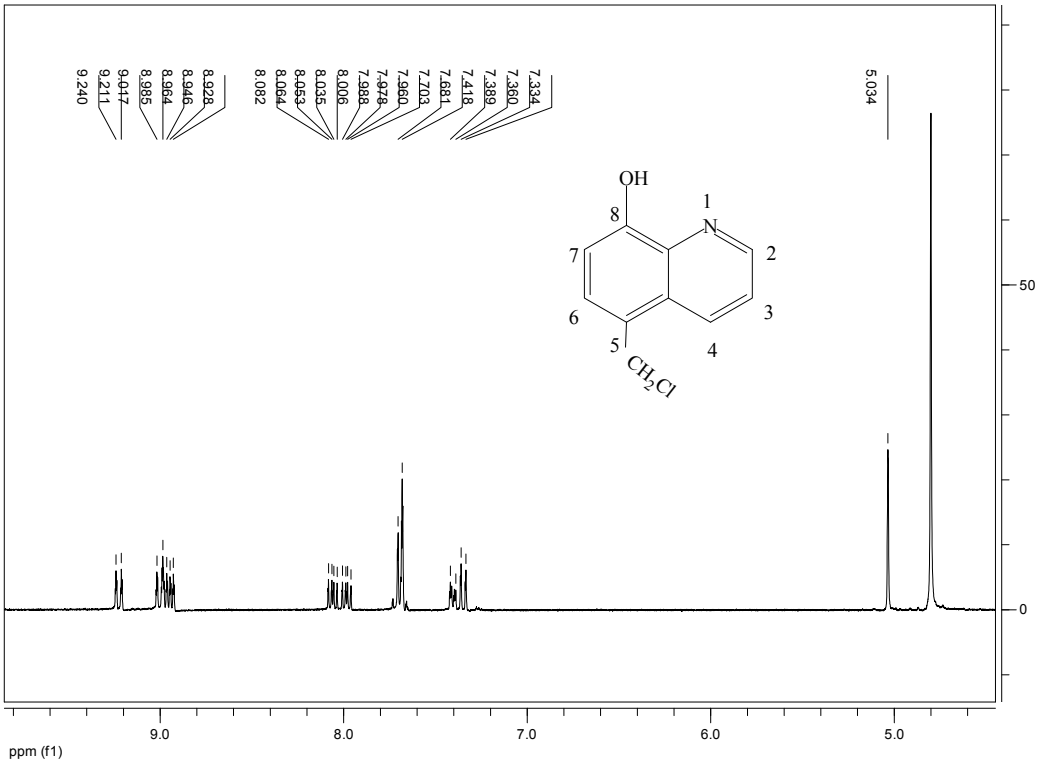


**Supplementary Figure S2.** $^{1}$H NMR spectrum of **1**.

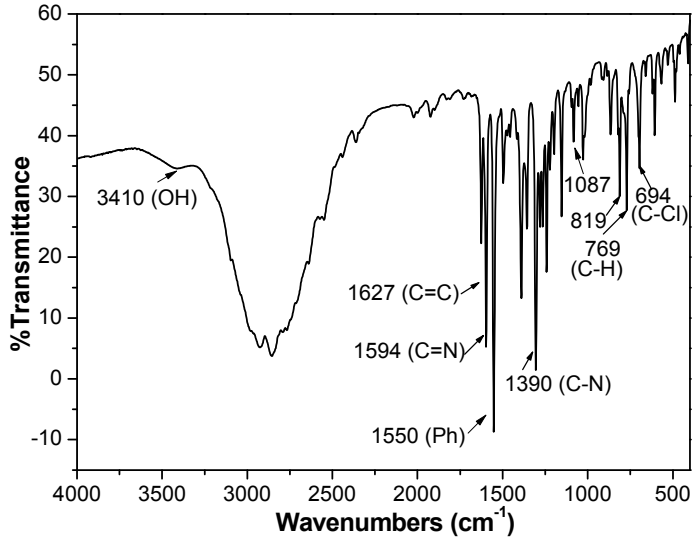


**Supplementary Figure S3.** FT-IR spectrum of **1**.

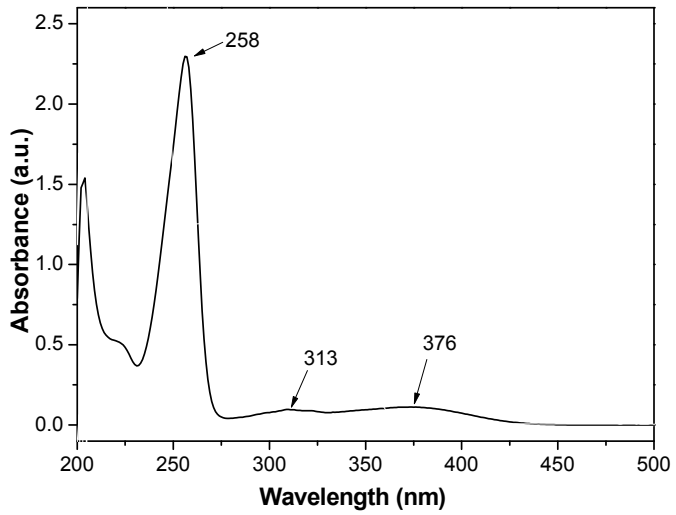


**Supplementary Figure S4.** UV-vis spectrum of **1**.

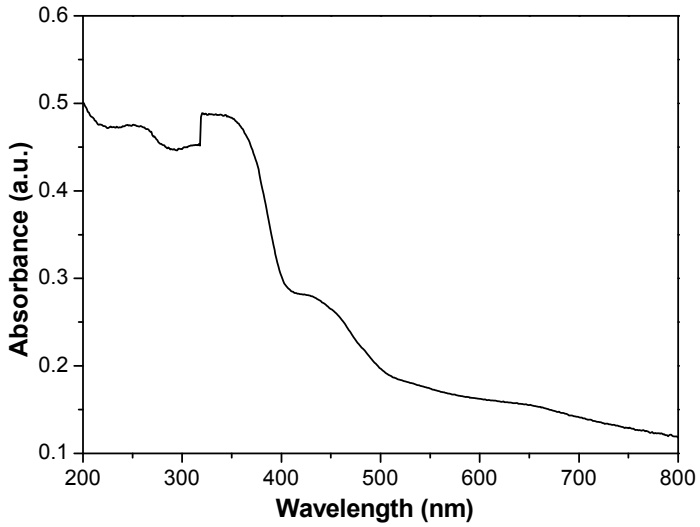


**Supplementary Figure S5.** UV-vis spectrum of CTS-HQ.

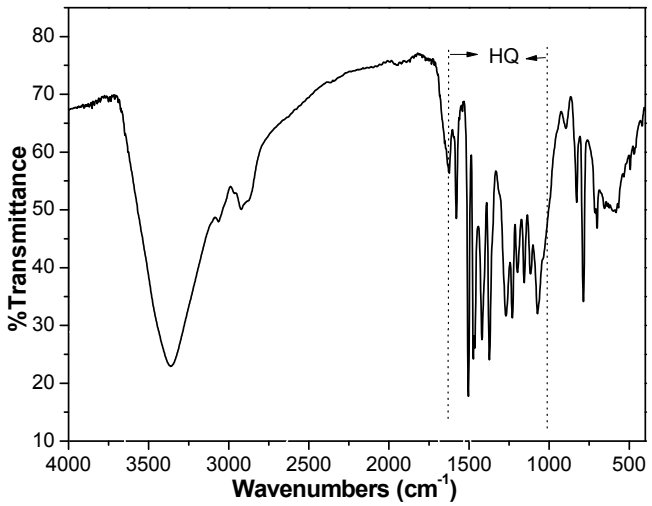


**Supplementary Figure S6.** FT-IR spectrum of CTS-HQ.

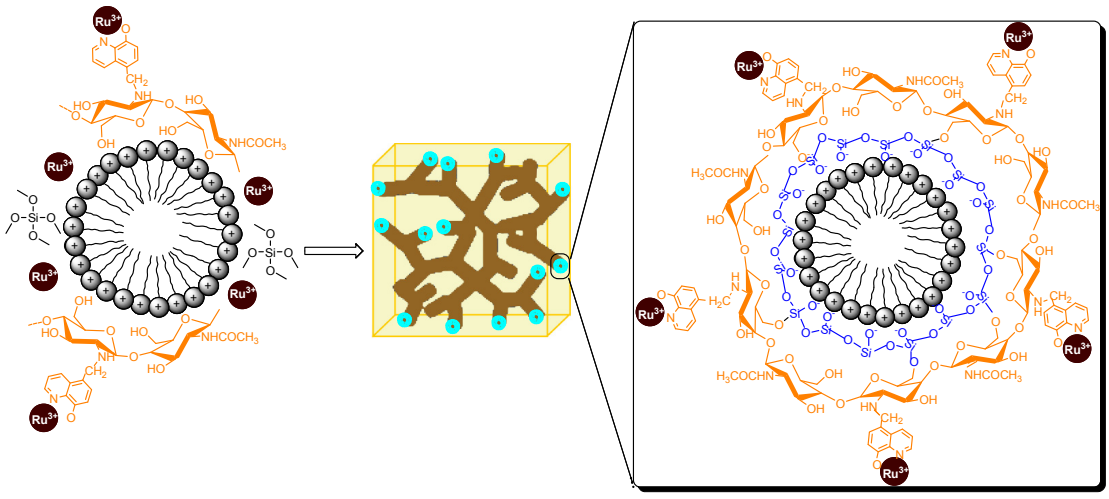

**Supplementary Figure S7.** Schematic illustrating of CTAB-directed multi-component self-assembly process. Note: some ions were obliterated for clarity.

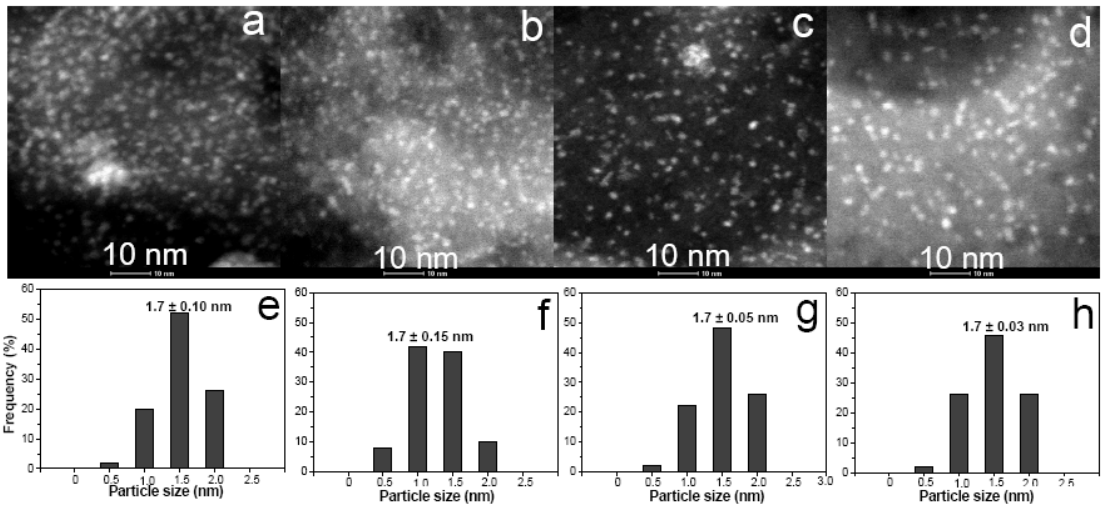


**Supplementary Figure S8.** HAADF images and the corresponding particle size distributions for (a,e) 6.0%Ru-OMC, (b,f) 3.0%Ru-OMC, (c,g) 1.5%Ru-OMC and (d,h) 0.5%Ru-OMC.

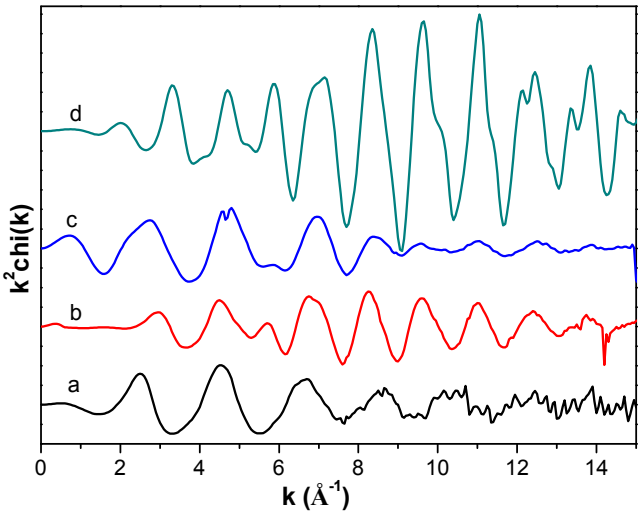


**Supplementary Figure S9.** Normalized EXAFS (Ru K-edge scan) plotted as $k^2$chi(k) *vs* k for (a) 3.0%Ru-$C_{16}$SC, (b) 3.0%Ru-OMSC, (c) 3.0%Ru-OMC and (d) Ru foil.

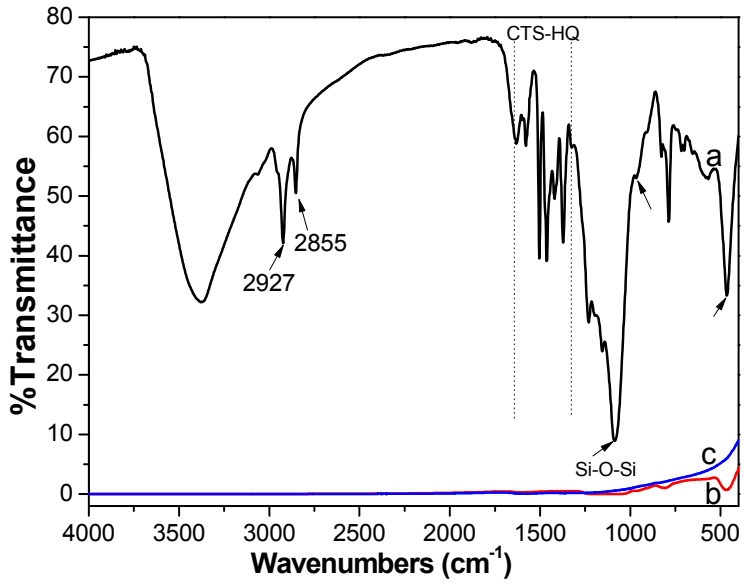


**Supplementary Figure S10.** FT-IR spectra of (a) 3.0%Ru-$C_{16}$SC, (b) 3.0%Ru-OMCS and (c) 3.0%Ru-OMC.

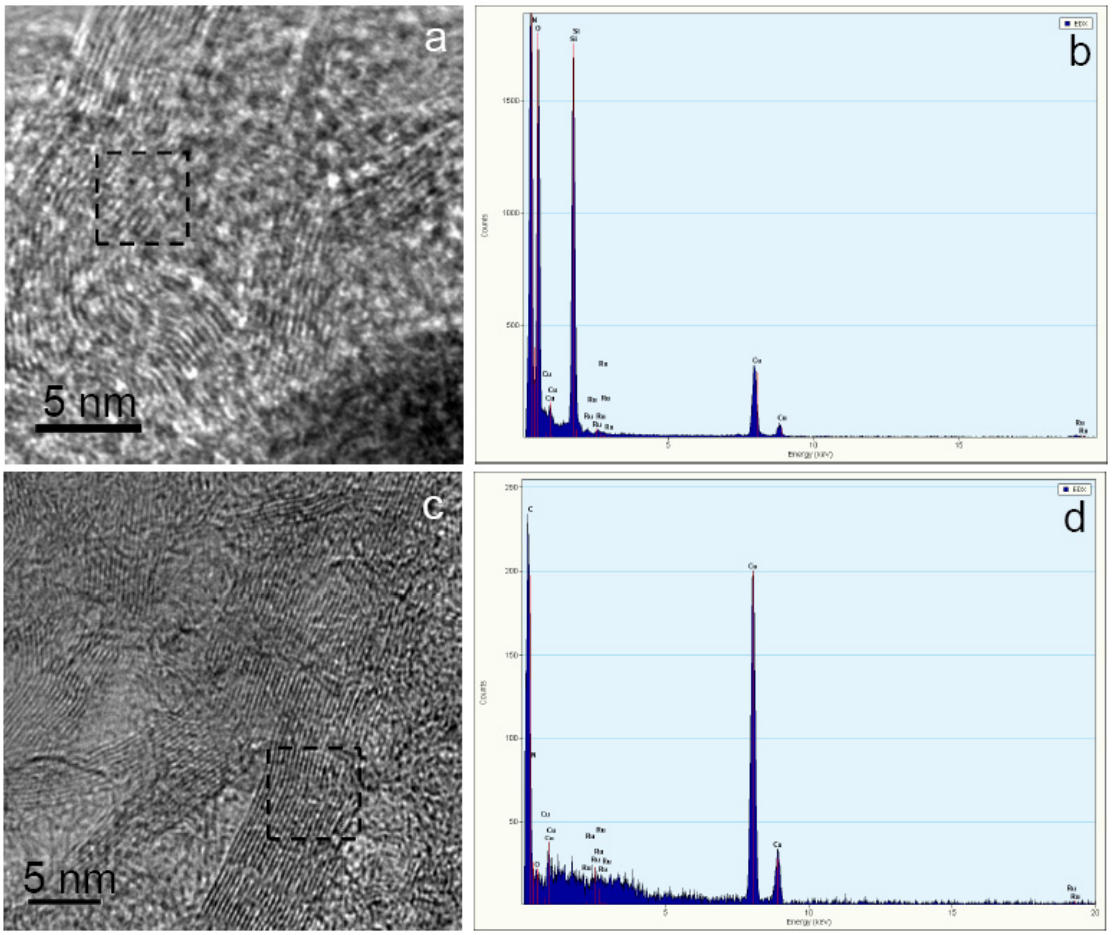


**Supplementary Figure S11.** TEM images and the corresponding EDX results for (a,b) 3.0%Ru-OMSC and (c,d) 3.0%Ru-OMC.

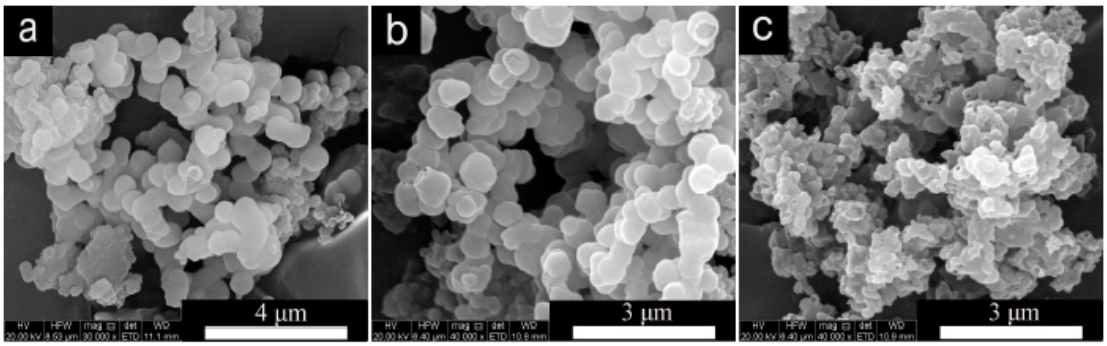


**Supplementary Figure S12.** SEM images of (a) 3.0%Ru-$C_{16}$SC, (b) 3.0%Ru-OMCS and (c) 3.0%Ru-OMC.

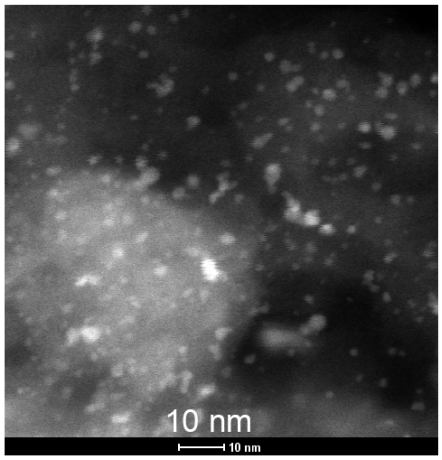


**Supplementary Figure S13.** Typical HAADF image of 3.0%Ru-OMC after 23 cycles.